

High efficiency of the lead methanesulfonate flow battery achieved by changing the characteristics of PbO_x under potentiostatic conditions

Xiaofei Luo, Zheng Liu*, Bailing Jiang, Dongdong Ji

School of Materials Science and Engineering, Xi'an University of Technology, No. 5 Jinhua South Road, Xi'an, 710048, China

ARTICLE INFO

Keywords:

Lead methanesulfonate flow battery
Potentiostatic conditions
Impedance
Coulombic efficiency

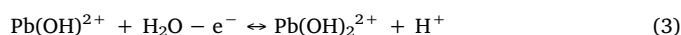
ABSTRACT

To investigate the deposition and dissolution of the anodic deposited materials in the lead methanesulfonate flow battery, phase composition, grain and particle sizes, stoichiometry and conductivity of PbO_2 are investigated, which are deposited at different positive electrode potentials. With the positive electrode potential increasing, the content of α -phase increases compared with β -phase's by X-ray diffraction (XRD) analyses. Mean grain sizes are not apparently changed by calculation using Debye-Scherrer formula. But the particle sizes indeed become smaller with the positive electrode potential increasing, which are investigated using scanning electron microscope (SEM). Since the anodic deposited material is the compound in which oxygen deficiency in PbO_2 , X-ray photoelectron spectroscopy (XPS) is introduced to characterize the non-stoichiometry of PbO_2 deposited at four typical positive electrode potentials, 1.5, 1.7, 1.8 and 2.0 V vs. SCE. Here PbO_x is utilized to represent this kind of compound. The highest value of $x = 1.73 \pm 0.03$ in PbO_x is obtained at 2.0 V vs. SCE, only $x = 1.46 \pm 0.02$ for that electrodeposited at 1.5 V vs. SCE. It is also found that the polarization impedances of working electrodes covered by different PbO_x layers decrease with the electrodeposition potential of PbO_x increasing, which are 170, 37, 12 and 2.4 Ω respectively at 1.5, 1.7, 1.8 and 2.0 V vs. SCE. By controlling the cell charge voltage of 2.15 V, corresponding to the positive electrode potential of 1.7 V vs. SCE, 261 cycling numbers have been achieved at the discharging current density of 40 mA cm^{-2} with a coulombic efficiency of more than 80 %.

1. Introduction

In 2004, a single electrolyte and no membrane flow battery was proposed by Pletcher *et al.* [1,2]. The principle of battery is that the soluble Pb^{2+} is deposited onto the positive electrode and the negative electrode respectively to produce PbO_2 and Pb during charging, while the discharge is a just opposite process with the charge. For the negative electrode: $\text{Pb}^{2+} + 2e \rightleftharpoons \text{Pb}$, the kinetics of Pb^{2+}/Pb couple are rapid, and the ratio of deposition and dissolution is close to one. For the positive electrode: $\text{Pb}^{2+} + 2\text{H}_2\text{O} - 2e \rightleftharpoons \text{PbO}_2 + 4\text{H}^+$, the kinetics of $\text{PbO}_2/\text{Pb}^{2+}$ couple are slow with significantly overpotentials during the deposition and dissolution of PbO_2 [1]. With the charge/discharge cycling, many more PbO_2 layers are built up on the positive electrode, decreasing the efficiency of the battery and limiting its service life [3]. Apparently the oxidation activity of PbO_2 is one of most important factors influencing the efficiency of the battery. For the PbO_2 electrodeposition mechanism, Velichenko *et al.* analyzed the formation of lead dioxide compared methanesulfonate with perchloric and nitric acid solutions [4–6]. They proposed an electrodeposition mechanism of lead

dioxide is similar as those in perchloric and nitric acid solutions, except for the quantitative difference of PbO_2 , and which is described as followed:



At low overpotential, the electrodeposition rate of lead dioxide is determined by the Eq. (3). At high overpotential, it is controlled by the diffusion rate of Pb^{2+} . As we have known, for metal oxide, the crystal phase is one of factors affecting the electrochemical activity of PbO_2 . In most PbO_2 deposits, there are two kinds of crystal phases, α - PbO_2 and β - PbO_2 . α - PbO_2 has a compact structure in a large size, and its electrochemical activity is low. Contrarily, β - PbO_2 has a loose structure in a small size, exhibiting relatively high electrochemical activity [7,8]. Li *et al.* prepared pure α - PbO_2 , β - PbO_2 and their mixtures in the

* Corresponding author.

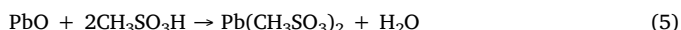
E-mail address: zhengliu@xaut.edu.cn (Z. Liu).

methanesulfonate media under the certain electrodeposition conditions, and the high columbic efficiency was achieved more than 20 cycles [9,10]. With continued cycling, the lead dioxide would be re-sidated and accumulated layer by layer. This indicates that α -/ β - PbO_2 is one of factors influencing the battery efficiency. Ouryet *et al* assessed the electrodeposition/dissolution cycling of PbO_2 by changing the concentrations of active species Pb^{2+} and H^+ [11]. They found that the non-stoichiometric PbO_x ($1 \leq x \leq 2$) compound could be formed during discharging, especially at the high content of H^+ . Due to its poor solubility and high electric resistance, the lead dioxide layer could be passivated to worsen the battery properties, especially at the high current density. This suggests that the content of O in the positive deposited materials, i.e. x value in PbO_x , influences the oxidation activity of PbO_x . In addition, when x varies from 1 to 2, PbO_x changes from an insulator (x close to 1) to a conductor (x close to 2), x is at least more than 1.5 [12]. During the charge, according to the above electrodeposition mechanism of PbO_2 , the anodic electrodeposited materials might not be 100% of PbO_2 , there must be existence of oxygen deficiency. It has been confirmed by Pavlov *et al.* and Suffredini *et al* [12–16].

To clarify the characteristics of PbO_x during charging in the electrolyte of lead methanesulfonate, the potentiostatic method was applied to investigate the content of O in the lattice ($\text{O}_{\text{lattice}}$) of positive electrodeposited materials in this work. The electrodeposition potentials were selected from the typical positive electrode potential vs. time response for constant current charge/discharge cycle. X-ray diffraction (XRD) was introduced to study the effects of the crystal phase and mean grain size on the discharge capacity of anodic deposited materials. Scanning electron microscope (SEM) was applied to image the surface morphology, and measure the particle size of PbO_x and its distribution. X-ray photoelectron spectroscopy (XPS) was performed to investigate the non-stoichiometry of PbO_x . The polarization impedance of the anodes predeposited with PbO_x layers at different positive electrode potentials were measured using an Electrochemical Impedance Spectroscopy (EIS).

2. Experimental

All solutions were prepared with the deionized water ($\ll 1 \mu\text{S cm}^{-1}$), the methanesulfonic acid (Chengdu KeLong Chemical Co. Ltd., 98 wt%), lead oxide (Tianjin Fuchen Chemicals Reagent Factory, 99 wt%) by the following reaction:



In this paper, the concentrations of methanesulfonic acid in all solutions were the residual acid concentration after the reaction with the lead oxide.

The charge/discharge cycles of flow cells were carried out by a Neware Battery Tester (Neware Technology Ltd, Shenzhen, China) in a solution containing 1.0 M $\text{Pb}(\text{CH}_3\text{SO}_3)_2$ + 1.0 M $\text{CH}_3\text{SO}_3\text{H}$ with a volume of 120 mL at 298 K. The electrolyte was filled into a glass beaker with an inner diameter of 5.6 cm and a height of 8 cm, which was stirred with a PTFE coated cylindrical magnetic bar at a speed of 200 rpm. The magnetic bar was placed at the center bottom of beaker, whose length and diameter were 2.8 cm and 0.9 cm respectively. The test was carried out in the same undivided beaker cell. The cell was fitted with two home-made electrodes (1.0 cm \times 1.0 cm \times 0.4 cm), whose conductivities were 12.34 S/cm. The home-made electrode was the carbon based filler/high density polyethylene (HDPE) composite plate. The carbon based fillers were including natural flake graphite (FG), carbon black (CB), and short carbon fiber (CF), which were supplied from Qingdao Rocksea Carbon Materials Co. Ltd (China). HDPE powder was supplied from Kunshan Hao Jia Plastic Products Co. Ltd (China). Its molecular weight is more than 1500,000, the density is 0.954 g/cm³, and the melting point is 142 °C from DSC analyses.

Carbon based fillers were mixed with HDPE powder in a weight ratio of FG : CB : CF : HDPE = 42.8 : 13.2 : 4 : 30 for 30 mins at 190 °C using an internal mixer (Lina Machinery Industrial Co. Ltd. (China)). Once cooling down to 150 °C, the mixture was moved to a 150 °C preheating two roll mill (Lina Machinery Industrial Co. Ltd. (China)) to produce a prepreg sheet. Finally the conductive composite plate was produced using a hot pressing machine (Shenzhen Superb Co. Ltd. (China)) with a pressure of 6 kgf/cm² at 190 °C. The copper plate with a size of 1.0 cm \times 1.0 cm \times 0.1 mm was used as a current collector. A copper cable as a current contact and electrode holder was welded in the center of the copper plate. A silver powder conductive adhesive (Wuhan Double-bond Chemical Co. Ltd (China)) was applied to stick the current collector and the electrode together, which was cured at 50 °C for 6 h with a pressure of 0.25 kgf/cm². After that the electrode, the copper plate and the welding point of the copper cable were covered with epoxy resin (Nantong Xingchen Synthetic Material., Ltd (China)), only an active area of 1.0 cm \times 1.0 cm of electrode was exposed. The epoxy resin was cured at 120 °C for 1 h, to protect the copper collector and silver powder conductive adhesive from corroding in the electrolyte. Finally the surface of carbon/HDPE electrode was polished using a 1000-grit papers, and acetone was used to clean the surface of the electrode to remove any contaminants, followed by rinsing with three batches of freshly deionized water to remove the excess acetone. In order to prevent short circuit from the formation of lead dendrite on the negative electrode, the inter-electrode gap was 2.0 cm. Two electrodes were immersed into the electrolyte with a depth of 1.5 cm below the liquid level, and the electrolyte flow rate across the electrode surface was around 21 cm/s.

Linear sweep voltammetry (LSV), was carried out using an electrochemical workstation (CHI660E, Shanghai, China), which was controlled by PC. The three electrode system was applied in the test. The working electrode was the home-made carbon/HDPE plate. Before each test, the working electrode was polished with 1000-grit papers, and orderly rinsed with acetone and the deionized water three times to remove any residuals. Its thickness was around 0.4 cm, the surface area was 1.0 cm \times 1.0 cm. The counter electrode was Pt (99.99%) provided by Shanghai Yueci electron technology Co., Ltd (China). The saturated calomel electrode was used as the reference with $\phi^0 = 0.241$ vs. NHE at 298 K, which was supplied from Luosu Science and Technology Co., Ltd (China). The initial potential of LSV was set to 1.4 V vs. SCE, and the final potential was fixed at 1.95 V vs. SCE. The concentration of electrolyte was 0.1 M $\text{Pb}(\text{CH}_3\text{SO}_3)_2$ + 1.0 M $\text{CH}_3\text{SO}_3\text{H}$. The volume was 120 mL, and the temperature was 298 K.

EIS was also carried out by the CHI660E. The working electrode was the home-made carbon/HDPE plate covered with PbO_x deposited at different positive electrode potentials. The counter electrode and the reference electrode were the same as the mentioned above. The electrochemical impedance was measured at the open circuit potential (1.3 V vs. SCE). Spectra were obtained in the frequency range of 10^{-2} Hz to 10^5 Hz with an AC amplitude of 10 mV at 298 K. The concentration of electrolyte was 1.0 M $\text{Pb}(\text{CH}_3\text{SO}_3)_2$ + 1.0 M $\text{CH}_3\text{SO}_3\text{H}$ with a volume of 120 mL.

XRD data were collected using a CONTURA G2 (Japan) X-ray diffractometer with Ni-filtered $\text{Cu K}\alpha$ radiation. The scan range was 20°–80°, and the scan rate was $10^\circ \text{ min}^{-1}$.

The morphologies of PbO_2 deposited at different positive electrode potentials were imaged by SEM (JSM-6700 F, Japan) with a voltage of 20 kV.

The chemical states of PbO_2 were investigated by XPS (AXISULTRA, Kratos, UK). XPS spectra were obtained with monochromatic Al $\text{K}\alpha$ (1486.71 eV) line at a power of 100 W (10 mA, 10 kV) with a vacuum of about 10^{-8} Torr. The charge neutralizer was used to compensate for surface charge effects, and binding energies were calibrated in a reference to the C1s hydrocarbon peak, 284.8 eV.

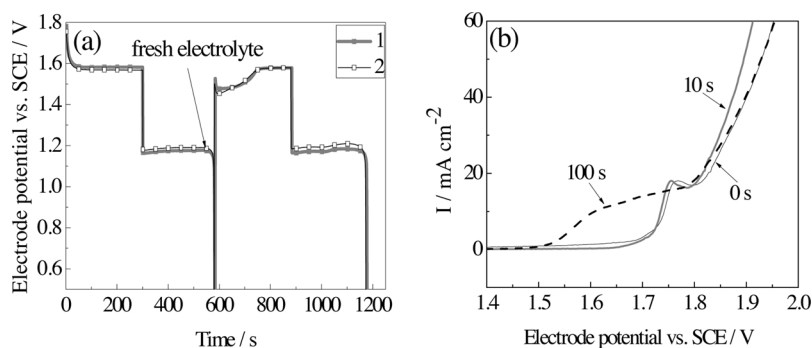


Fig. 1. (a) 1st, 5th, 10th, 100thth Charge-discharge plots of the first 10 times and (b) the 1st, 5th, 10th, 100th charge curves. The cell was charged for 2 h and then discharged at the same current density of 10 mA cm^{-2} until the cell voltage dropped to 0.5 V. Electrolyte: $1.0 \text{ M Pb}(\text{CH}_3\text{SO}_3)_2 + 1.0 \text{ M CH}_3\text{SO}_3\text{H}$. Temperature: 298 K.

3. Results and discussions

3.1. Characteristics of constant current charge/discharge cycles

A charge-discharge curve was obtained at the current density of 10 mA cm^{-2} in an electrolyte containing $1.0 \text{ M Pb}(\text{CH}_3\text{SO}_3)_2 + 1.0 \text{ M CH}_3\text{SO}_3\text{H}$ (Fig. 1(a)). It can be seen that the cell charge voltage varies during cycling. In Fig. 1(b), 1st, 5th, 10th, 100th the cell charge voltage becomes obviously lower with the cycling number, $1^{\text{st}} > 5^{\text{th}} > 10^{\text{th}} > 100^{\text{th}}$. This indicates that the driving force required for the nucleation of PbO_2 on the fresh electrode is larger. Coulombic efficiency of the 1th, 5th, 10th and 100th cycles are 90%, 94%, 95% and 83% respectively. The cell charge voltage, especially the initial charge voltage in the cycles, gradually becomes lower than the first cycle's. This shows that there are some advantages, by which the properties of PbO_2 must be improved. The promotion for the electrodeposition of PbO_2 could be attributed to the properties of electrolyte, such as the concentrations of active species, Pb^{2+} and H^+ , or the surfacial properties of the electrodes, such as the properties of anodic deposited materials. Pletcher and Wills reported that the lead(II) oxide could be arised during the dissolution of PbO_2 , if the concentration of Pb^{2+} in the boundary layer close to the electrode became high enough to exceed the solubility product of a lead(II) species, which would be reoxidized back to PbO_2 more readily than that in solution [2].

In order to avoid the influence of the concentrations of Pb^{2+} and H^+ , the electrolyte was changed after the first charge/discharge cycle. The curves of the positive electrode potential as a function of time were recorded during the deposition and dissolution of PbO_2 at the current density of 10 mA cm^{-2} (Fig. 2(a)). The grey Line 1 is a V-t curve of two charge-discharge cycles in the same electrolyte at the first test. It can be seen that the initial positive charge potential is higher, almost 1.75 V vs. SCE during the first charging process. Once PbO_2 is nucleated, its electrodeposition is promoted significantly, the charge potential drops to a steady value of $\approx 1.60 \text{ V}$ vs. SCE. The second charge curve is clearly different from the first charge curve, the positive electrode potential is lower at the beginning charge, and it gradually rises to $\approx 1.60 \text{ V}$ vs. SCE as the charge proceeds. In order to avoid the influence of electrolyte, another two charge/discharge cycles were performed again using the same fresh electrolyte. After the first cycle, the electrolyte was changed again with the fresh one, whose composition was the same as that in the first cycle, as shown in the black Line 2. There is a slight difference of the charge and discharge potentials between Line 1 and Line 2. Similarly two charging curves become stable at the same stage in these two procedures. Therefore, in the initial stage of the second charge, the promotion for the electrodeposition of PbO_2 has nothing to do with the concentration of Pb^{2+} or H^+ . It must be related to the surfacial properties of the electrode [3]. After the first cycle, the residual PbO_2 reduces the interfacial energy of nucleation, lowering the tentio electrodeposition potential of PbO_2 .

To clarify the above conclusion, LSV was performed in the rage of $1.4 \sim 1.95 \text{ V}$ vs. SCE, as shown in Fig. 2(b). Firstly the home-made carbon/HDPE electrodes were electrochemically deposited with PbO_2

at the current density of 5 mA cm^{-2} for different times, 0 s, 10 s and 100 s. It can be seen from the diagram, the oxidation peak of PbO_2 is about 1.7 V vs. SCE for the fresh electrode. It shifts negatively about 0.02 V for the electrode predeposited with a PbO_2 layer for 10 s. When the pre-deposition time of PbO_2 is 100 s, the oxidation peak potential shifts negatively to about 1.55 V vs. SCE. The initial deposition potential of PbO_2 decreases significantly. The oxidation peak is broadened, and the range of deposition potential of PbO_2 is enlarged. So it could be inferred that the initial oxidation potential of PbO_2 was lowered by the existence of PbO_2 in the following charging cycles.

3.2. Effect of positive electrode potential on the deposition/dissolution of PbO_2

During the constant current charge/discharge cycling, the cell charge voltage decreased with the number of cycles due to the residual PbO_2 . PbO_2 is more or less resided after discharge, which has been found by many researchers [9,17,18]. The cell voltage inevitably varies in different constant current charging processes. Therefore, it is necessary to study the effects of different positive electrode potentials on the discharge capacity of PbO_2 . Fig. 3 shows that the cells are charged to the capacity of 0.28 mAh^{-} at different positive electrode potentials, and discharged at different current densities, 2, 10, 20 and 40 mA cm^{-2} . In Fig. 3(a), discharge capacities of PbO_2 deposited at different potentials are different at 2 mA cm^{-2} . When the positive electrode potential is less than 1.8 V vs. SCE, the discharge capacity of PbO_2 was generally enhanced with the electrodeposition potential increasing, even though the oxygen evolution phenomena was observed at 1.8 V vs. SCE. This shows that the activity of PbO_2 is improved by the high positive electrode potential. When the positive electrode potential is 2.0 V vs. SCE, the severe oxygen evolution occurred during charging to decrease the charge efficiency, lowering the discharging capacity. The same results were observed at other discharging current densities, 10, 20 and 40 mA cm^{-2} (Figs. 3(b)-3(d)). It can be concluded that the oxidation activity of PbO_2 is improved by the high positive electrode potential. However the oxygen evolution reaction could occur at the high positive electrode potential during the electrodeposition of PbO_2 that would lower the efficiency of cell.

For the electrodeposited PbO_2 film, mostly it is a mixture of α -phase and β -phase [9,19]. To investigate the relationship between the discharging capacity of PbO_2 and the crystal phase, XRD was introduced to characterize phase compositions of PbO_2 deposited at different positive electrode potentials, as shown in Fig. 4. At all different potentials, there are mixed α - and β -phases existed in the electrodeposition PbO_2 . With the positive electrode potential increasing, the content of α -phase increases along with β -phase's decreasing. The same result has been reported by many researchers through increasing the charging current density [4,9,20]. The current density is large at the high positive electrode potential in this work. Average grain sizes have been calculated by Debye-Scherrer formula based on typical lattice planes, α - PbO_2 (020) & (002) and β - PbO_2 (211) & (301) [21,22], as listed in Table 1. Mean grain sizes of PbO_2 are not obviously changed at different

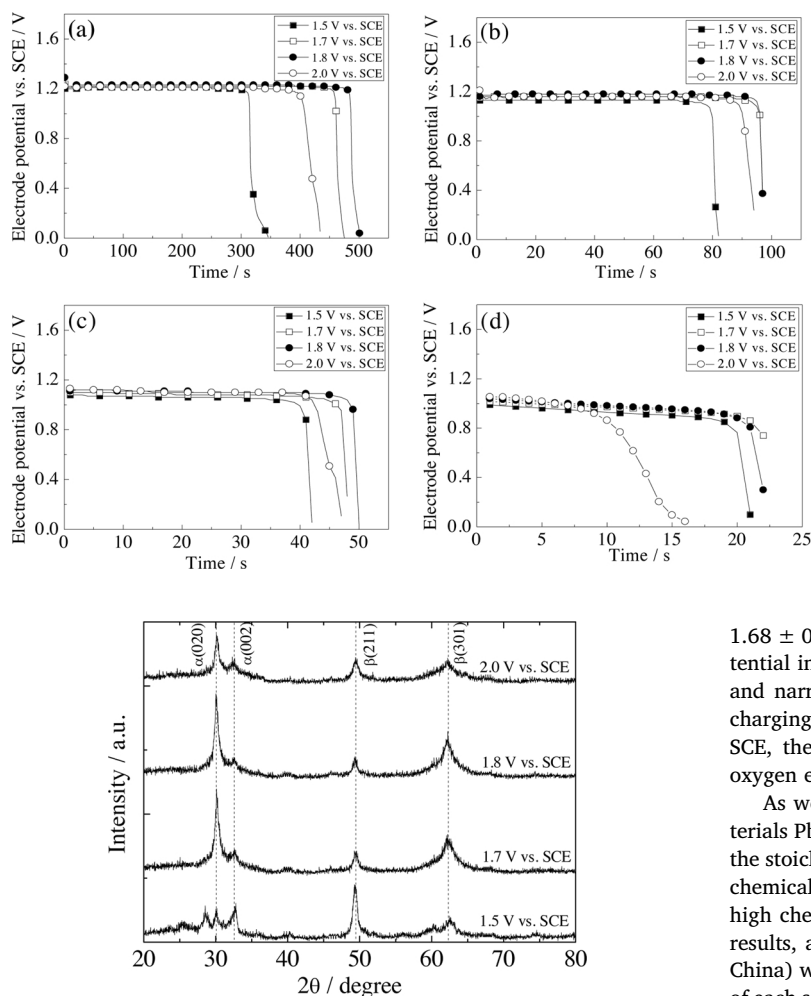


Fig. 3. (a) $2 \text{ mA}\cdot\text{cm}^{-2}$; (b) $10 \text{ mA}\cdot\text{cm}^{-2}$; (c) $20 \text{ mA}\cdot\text{cm}^{-2}$; (d) $40 \text{ mA}\cdot\text{cm}^{-2}$; (e) $10 \text{ mA}\cdot\text{cm}^{-2}$; (f) $20 \text{ mA}\cdot\text{cm}^{-2}$; (g) $40 \text{ mA}\cdot\text{cm}^{-2}$ Positive electrode potential vs. time curves of PbO_2 deposited at different potentials during discharging at different current densities (a) $2 \text{ mA}\cdot\text{cm}^{-2}$; (b) $10 \text{ mA}\cdot\text{cm}^{-2}$; (c) $20 \text{ mA}\cdot\text{cm}^{-2}$; (d) $40 \text{ mA}\cdot\text{cm}^{-2}$. All cells were charged to $0.28 \text{ mA}\cdot\text{h}$ and then discharged until the positive electrode potential dropped to 0 V vs. SCE. Electrolyte: $1.0 \text{ M Pb}(\text{CH}_3\text{SO}_3)_2 + 1.0 \text{ M CH}_3\text{SO}_3\text{H}$. Temperature: 298 K .

potentials, except for the grain size of $\alpha\text{-PbO}_2$ (020) deposited at 1.5 V vs. SCE being larger than others. Generally $\beta\text{-PbO}_2$ has a better electrochemical performance than $\alpha\text{-PbO}_2$ that has been reviewed by Krishna *et al* [3]. However, with the positive electrode potential increasing, the content of $\alpha\text{-PbO}_2$ increased, the discharge capacity was enhanced. It is difficult to conclude that the discharging capacity has been only affected by the crystal phase and the grain size of PbO_2 , which are deposited at different positive electrode potentials 1.5 , 1.7 , 1.8 and 2.0 V vs. SCE.

To further investigate the effect of particle size of PbO_2 on the discharge capacity, it is necessary to image the surface morphologies of PbO_2 deposited at different positive electrode potentials using SEM Fig. 5. —The particle sizes were measured utilizing an ImageJ software to obtain their average value and size distributions, as shown in Figs. 5(a)–5(d). At the positive electrode potential of 1.5 V vs. SCE, the size distribution of PbO_2 particles is from 1.6 to $3.8 \mu\text{m}$, and their average size is $2.48 \pm 0.52 \mu\text{m}$. When the deposited potential increases to 1.7 V vs. SCE, the size distribution of PbO_2 particles is from 1.2 to $2.6 \mu\text{m}$, and their average size is $1.88 \pm 0.27 \mu\text{m}$. When the positive electrode potentials increase up to 1.8 and 2.0 V vs. SCE, the size distributions of PbO_2 particles become narrower, 1.05 – $2.2 \mu\text{m}$ and 1.0 – $2.15 \mu\text{m}$ respectively, and their corresponding average sizes are

Fig. 2. (a) — Positive electrode potential vs. time plots during the deposition and dissolution of PbO_2 . The cells were charged for 300 s and then discharged at the same current density of $10 \text{ mA}\cdot\text{cm}^{-2}$ until the positive electrode potential dropped to 0.5 V vs. SCE. (b) LSV curves of the carbon/HDPE electrode predeposited with PbO_2 at the current density of $5 \text{ mA}\cdot\text{cm}^{-2}$ for different times 0 s , 10 s and 100 s . The scan rate: $5 \text{ mV}\cdot\text{s}^{-1}$. Temperature: 298 K .

$1.68 \pm 0.25 \mu\text{m}$ and $1.58 \pm 0.26 \mu\text{m}$. With the positive electrode potential increasing, the particle size and its distribution become smaller and narrower, favoring the dissolve of PbO_2 and increasing the discharging capacity. But for the positive electrode potential of 2.0 V vs. SCE, the amount of deposited PbO_2 was lowered due to the severe oxygen evolution reaction.

As we have known, the oxidation activity of anodic deposited materials PbO_x ($1 \leq x \leq 2$) depends on the oxidation state of lead ion and the stoichiometry of PbO_x [23–25]. XPS was applied to characterize the chemical state of PbO_x . The high O content of crystal PbO_x means the high chemical valence of lead ion. In order to guarantee the accurate results, a reference specimen of PbO_2 (supplied from J&K[®] Company, China) was scanned, as show in Fig. 6(a). And also five different areas of each sample were selected to measure the ratio of O : Pb. The average x value of the reference sample is 1.99 ± 0.01 , which is satisfied with the reference data, 1.99 , provided by the supplier. Fig. 6(b)–(e) show the XPS narrow scans of elemental O of different electrodeposited PbO_x . In all PbO_x films deposited at different positive electrode potentials, there are three peaks of O. The 529.00 eV peak is attributed to O in the crystal PbO_x ($\text{O}_{\text{lattice}}$). The O peak of 531.50 eV might be attributed to the hydrated $\text{PbO}(\text{OH})_2$, or the air/ O_2 [15], which is marked using $\text{O}_{\text{adsorption}}$. The O peak of 532.80 eV is attributed to H_2O [24,26]. With the positive electrode potential increasing, the content of $\text{O}_{\text{lattice}}$ correspondingly increased. By semi-quantitative calculation, the ratio of O : Pb does not obeyed the stoichiometric ratio of $2:1$. The ratio of O : Pb is 1.46 ± 0.02 for PbO_x deposited at 1.5 V vs. SCE, i.e. $x = 1.46 \pm 0.02$. When the positive electrode potential is 2.0 V vs. SCE, $x = 1.73 \pm 0.03$. According to Velichenko *et al*'s proposal of electrodeposition mechanism of PbO_2 , in the first stage, $\text{OH}_{\text{adsorption}}$ is firstly produced by the activation of the solvent H_2O (Eq. (1)), which would be combined with Pb^{2+} to form the intermediate product, $\text{Pb}(\text{OH})^{2+}$, continued to combined with $\text{OH}_{\text{adsorption}}$ to produce $\text{Pb}(\text{OH})_2^{2+}$, which is decomposed chemically to form PbO_2 . Based on XPS results, the ratios of O : Pb are 1.46 ± 0.02 , 1.52 ± 0.01 , 1.61 ± 0.02 and 1.73 ± 0.03 in PbO_x deposited at different positive electrode potentials, 1.5 , 1.7 , 1.8 and 2.0 V vs. SCE, respectively. The oxygen deficiency must be existed in PbO_2 . It might be explained that the content of Pb(II) exceeded the solubility of the Soluble Pb(II) since the content of H^+ was low in the boundary layer close to the positive electrode under the function of electric field, which can be reacted with the active O from the activation of $\text{PbO}(\text{OH})_2$, or from the activation of OH^- [15–18]. Here, we can clarify that the positive active materials are the compound in which oxygen deficiency in PbO_2 . The x value is closed to 2, it means the oxidation activity of PbO_x is high, and good conductivity as well. At the high positive electrode

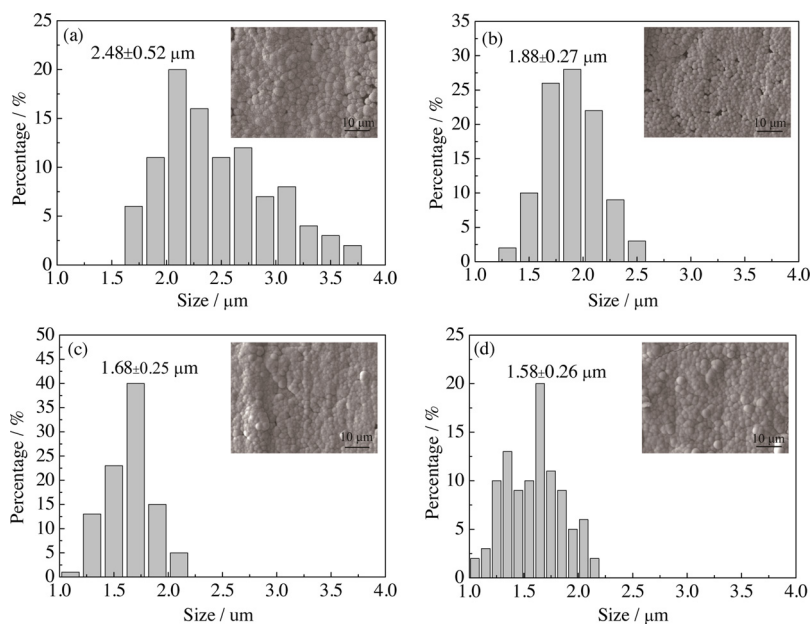


Fig. 4. XRD spectra of PbO_2 deposited at different positive electrode potentials.

potential, it is beneficial for the production of OH_{ads} , promoting the chemical reactions to the right of Eqs. (1)–(4), and contributing to the formation of PbO_2 . That is to say, the $\text{O}_{\text{lattice}}$ content of PbO_x deposited at the high positive electrode potential is correspondingly large.

Once PbO_x is electrochemically deposited onto the anode, the surfacial properties of the electrode would be changed, influencing the impedance of the cell. The electrodes were predeposited with PbO_x to the same charging capacity of 2.8 mA h at different positive electrode potentials in this work, which were used as the working electrodes. The impedance was measured at an open circuit potential. Fig. 7 represents the Nyquist plots obtained from PbO_x covered working electrodes using EIS. All the EIS curves are consisted of the capacitance arc at high frequency and the diagonal at low frequency. Nyquist plots were fit to a basic equivalent circuit model, as shown in Fig. 7. In this model, R_L represents the solution resistance, and C_d is the capacitance of the electric double layer closed to the electrode surface. R_p is the polarization resistance, which is related to the surface state variables of electrode, such as the overpotential E , the properties of PbO_x , and charge transfer resistance R_{ct} . R_w and C_w are the resistance and capacitance respectively, which are related to the diffusion rate of active species, i.e. the diffusion impedance $Z_w = R_w + C_w$. In this work, the compositions of all electrolytes were same, 1.0 M $\text{Pb}(\text{CH}_3\text{SO}_3)_2 + 1.0 \text{ M CH}_3\text{SO}_3\text{H}$. All tests were performed at the same open circuit, i.e. positive electrode potential was 1.3 V vs. SCE. It was too low, and we assumed that there was no any electron transfer to produce any new PbO_x layer. Therefore, R_L , E , R_{ct} , R_w and C_w are the same for all EIS measurements. R_p has mostly something to do with the properties of PbO_x pre-deposited at different positive electrode potentials. In Fig. 7, for the electrode covered with PbO_x at the low potential, the diameter of capacitance arc is large. However, it is small for the electrode covered with PbO_x deposited at the high potential. The polarization resistance,

R_p is decreased for the electrode with PbO_x deposited at the high potential. By fitting using Zview software, the values of R_p can be calculated, which are 170, 37, 12 and 2.4Ω respectively for the working electrodes covered with PbO_x layer pre-deposited at different positive electrode potentials, 1.5, 1.7, 1.8 and 2.0 V vs. SCE. R_p of the electrode with the high potential electrodeposition PbO_x is low. It must be related to properties of PbO_x on the surface of the electrode, such as the conductivity of PbO_x and its specific area. The conductivity of PbO_x was improved at the high positive electrode potential since x was close to 2 [12]. The corresponding specific area of the PbO_x layer on the electrode was large because the particle size of PbO_x was smaller than that deposited at the low potential (Fig 5). Therefore, these properties of PbO_x deposited at the high positive electrode potential would be beneficial for the charge transfer kinetics of $\text{Pb}^{2+}/\text{PbO}_2$. It can be well explained that at the high positive electrode potential, the small sized PbO_x is deposited onto the surface of the electrode to form a high conductive layer with a large specific surface area. The charge transfer kinetics is faster, favoring the nucleation of PbO_2 . Contrarily, at the low positive electrode potential of 1.5 V vs. SCE, the particle size of PbO_x is large, and its conductivity is poor due to $x < 1.5$ [12]. The charge transfer kinetics is relatively slow after the entire electrode surface is covered with PbO_x .

3.3. Cycling properties of the cell under potentiostatic conditions

Since the positive electrode potential varies under galvanostatic charging method, the content of $\text{O}_{\text{lattice}}$ in PbO_x must vary during the charge process. The oxidation activity of PbO_x are different between layer and layer. In order to guarantee the uniform oxidation activity of PbO_x , the constant charge voltage of the cell, 1.92, 2.15 and 2.27 V were applied to investigate the charge/discharge properties, to further

Table 1

Average grain sizes of PbO_2 deposited at different positive electrode potentials.

Positive electrode potential vs. SCE/ V trod	Average grain sizes of α - $\text{PbO}_2(020)/ \text{nm}$	Average grain sizes of α - $\text{PbO}_2(002)/ \text{nm}$	Average grain sizes of β - $\text{PbO}_2(211)/ \text{nm}$	Average grain sizes of β - $\text{PbO}_2(301)/ \text{nm}$
1.5	191	143	121	122
1.7	166	148	135	106
1.8	157	152	144	113
2.0	148	164	145	108

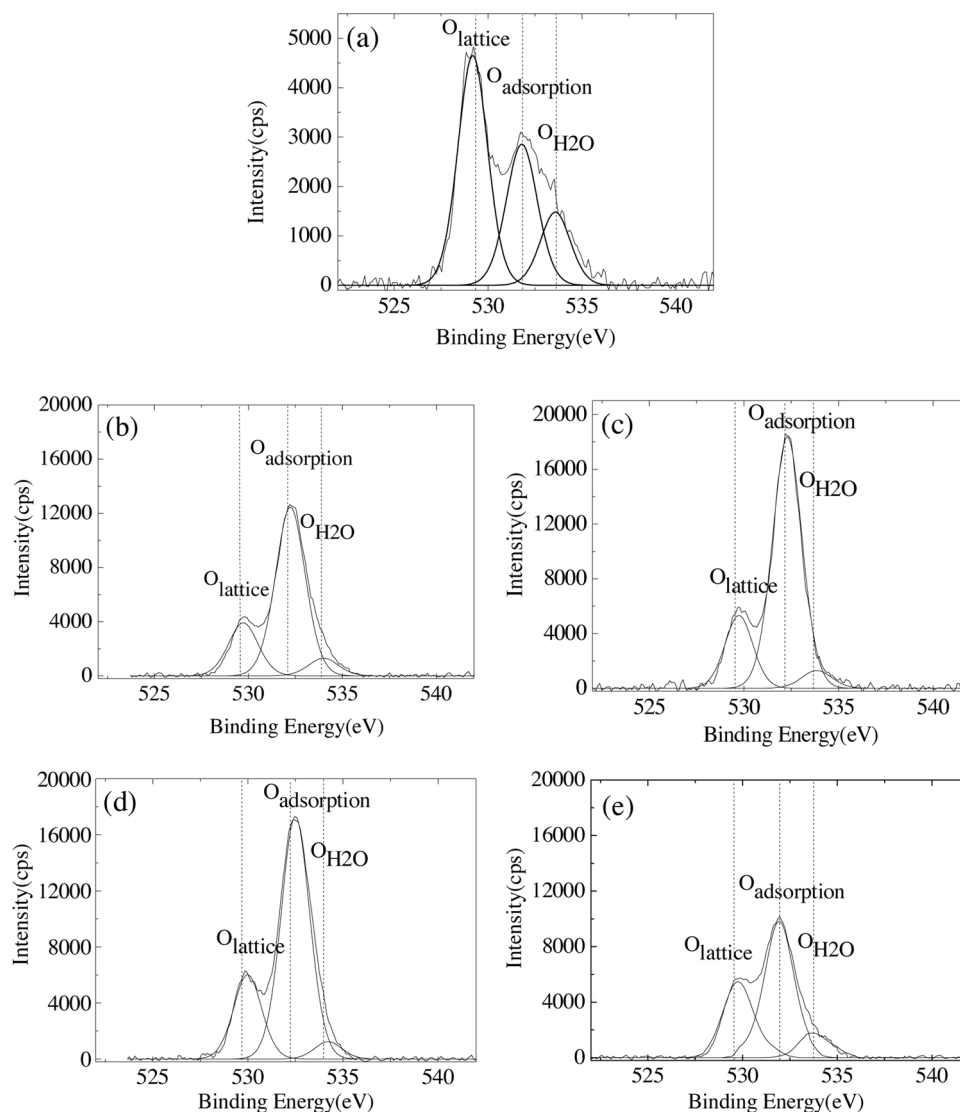


Fig. 5. Particle sizes and their distributions of PbO_2 deposited at different positive electrode potential. (a) 1.5 V vs. SCE, (b) 1.7 V vs. SCE, (c) 1.8 V vs. SCE, (d) 2.0 V vs. SCE.

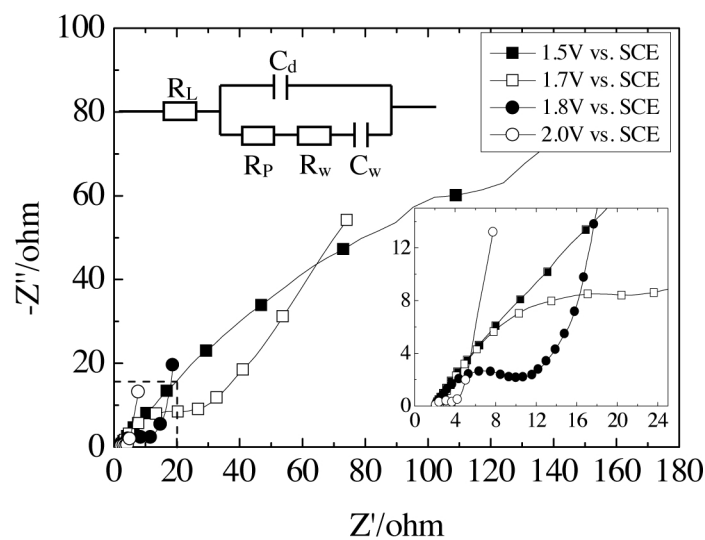


Fig. 6. XPS narrow scans of elemental O in PbO_2 , (a) Reference specimen PbO_2 , (b) PbO_x deposited at 1.5 V vs. SCE (c) PbO_x deposited at 1.7 V vs. SCE (d) PbO_x deposited at 1.8 V vs. SCE (e) PbO_x deposited at 2.0 V vs. SCE.

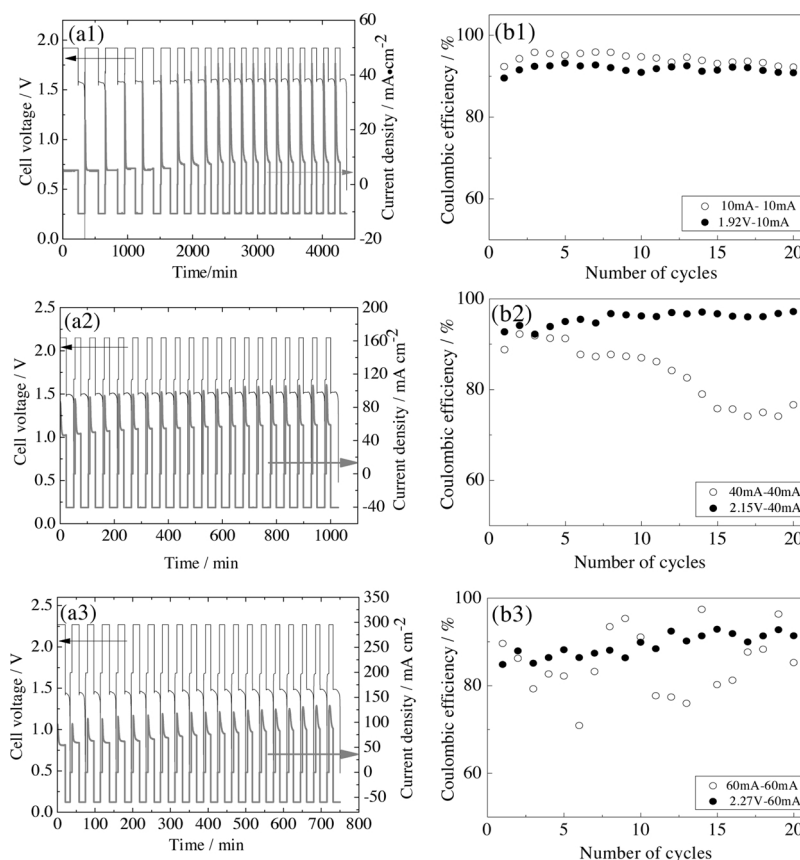


Fig. 7. Nyquist plots from EIS measurements for the electrodes at an open circuit voltage 1.3 V vs. SCE, the electrodes were pre-deposited with PbO_x at different positive electrode potentials 1.5, 1.7, 1.8 and 2.0 V vs. SCE, in the electrolyte of 1.0 M $\text{Pb}(\text{CH}_3\text{SO}_3)_2$ + 1.0 M $\text{CH}_3\text{SO}_3\text{H}$. Temperature: 298 K.

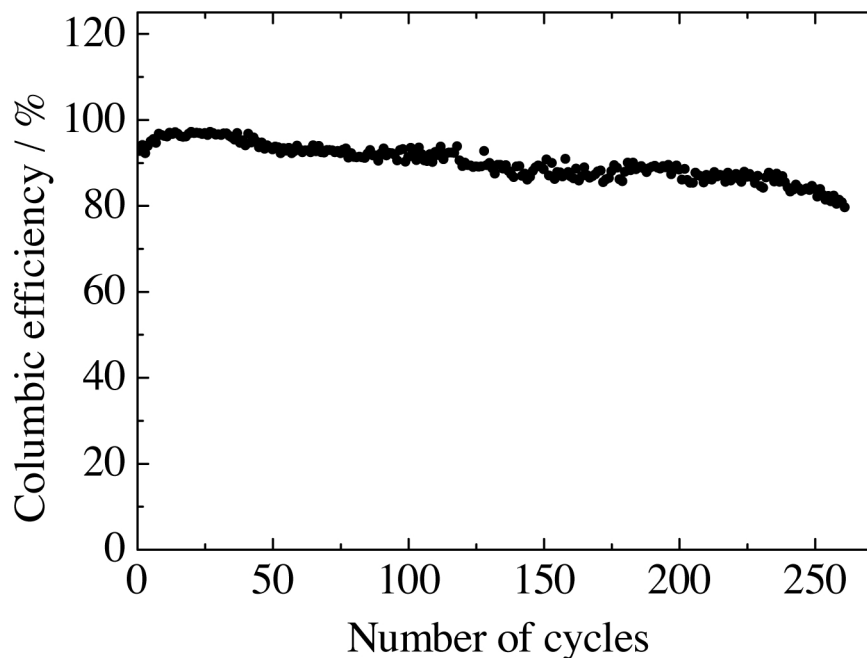


Fig. 8. --- Cycling properties of lead methanesulfonate flow cells under potentiostatic and galvanostatic conditions: (a1 - a3) The cell voltage (or current) vs. time data for 20 charge/discharge cycles, the cells were charged to 20 mA h at different voltages (a1) 1.92 V (a2) 2.15 V (a3) 2.27 V, and discharged at different current densities (a1) 10 mA cm^{-2} (a2) 40 mA cm^{-2} (a3) 60 mA cm^{-2} until the cell voltage dropped to 0.5 V; (b1 - b3) Coulombic efficiencies of lead methanesulfonate flow cells under potentiostatic and galvanostatic conditions, see the text for details of the regimes. Electrolyte: 1.0 M $\text{Pb}(\text{CH}_3\text{SO}_3)_2$ + 1.0 M $\text{CH}_3\text{SO}_3\text{H}$. Temperature: 298 K.

assess the potentiostatic and the galvanostatic methods. These voltages were chosen as they correspond to their positive electrode potentials 1.5, 1.7 and 1.8 V vs. SCE. In this work, all cells were cycled for 20 times, which were charged to the same capacity of 20 mA h at the cell voltages of 1.92, 2.15 and 2.27 V, and their corresponding discharging current densities were set to 10, 40, and 60 mA cm^{-2} until the cell

voltage dropped to 0.5 V (Fig. 8).

Fig. 8(a1) shows profiles of the cell voltage (or current) vs. time for 20 cycles of the cell, which was charged at 1.92 V and discharged at a current density is 10 mA cm^{-2} . Its charging current density at 1.92 V is ≈ 10 mA cm^{-2} . The average coulombic efficiency of the charge/discharge cycles at the same current density of 10 mA cm^{-2} (10 mA - 10

mA) is $93 \pm 2\%$ (Fig. 8 (b1)). It is better than that of the cell, $91 \pm 1\%$, which was charged at 1.92 V and discharged at 10 mA cm^{-2} (1.92 V - 10 mA) under potentiostatic conditions. This is because the charge voltage at the current density of 10 mA cm^{-2} under galvanostatic conditions was higher than 1.92 V, PbO_x exhibited a higher oxidation activity than that formed at 1.92 V.

Fig. 8(a2) shows the voltage (or current) vs. time behavior during the first 20 cycles of the lead methanesulfonate flow cell, which was charged at 2.15 V and discharged at 40 mA cm^{-2} (2.15 V - 40 mA). It can be seen that the charging current density at 2.15 V is $\approx 50 \text{ mA cm}^{-2}$. Its average coulombic efficiency is $94 \pm 2\%$ for 20 cycles (Fig. 8(b2)). When the cell is charged and discharged at 40 mA cm^{-2} (40 mA - 40 mA), its efficiency is lower and fluctuating. The fluctuation of efficiency has been presented in Collins *et al.*'s work using galvanostatic charging method [27]. It could be explained that the drop of PbO_x from the electrode into the electrolyte would reduce the discharging capacity of cell. It could be forced by the stress within the layer [28]. Contrarily the partial reoxidation of PbO_x into PbO_2 would reduce the amount of the passivated layer [11,17,29]. It would increase the conductive channels to favor the reduction of PbO_2 that cannot be further reduced in the previous cycling due to the impedance of the passivated layer, improving the discharging capacity. However, the new formed passivated layer would further decrease the discharging capacity. For PbO_x dropping off the anode, here we proposed another reason that might be related to the electrochemical activity of PbO_x . PbO_x deposited at different positive electrode potentials have different electrochemical activities. During the constant current charging, the positive electrode potential varies, so the electrochemical activities of PbO_x are different, the high oxidation PbO_x is firstly dissolved during discharging. It is possible to result in the drop of PbO_x with a low oxidation activity. When the cell is charged by the constant voltage, PbO_x with uniform electrochemical activity could be obtained, so its efficiency is more stable.

Fig. 8(a3) shows 20 charge/discharge cycles under potentiostatic conditions, in which the cell was charged at 2.27 V and discharged at 60 mA cm^{-2} (2.27 V - 60 mA). The current density at 2.27 V is $\approx 60 \text{ mA cm}^{-2}$. Fig. 8(b3) shows its average coulombic efficiency compared with that of cell charged and discharged at a current density of 60 mA cm^{-2} (60 mA - 60 mA). Their efficiencies are all low because of the oxygen evolution reaction. The black deposits were also observed at the bottom of the beaker. The efficiency of the cell charged at 2.27 V and discharged at 60 mA cm^{-2} is relatively stable, and that of the cell charged/discharged at constant current density is lower and fluctuating. It is mainly because that the charge voltage at 60 mA cm^{-2} is higher than 2.27 V, more severe oxygen evolution reaction happens to lead to the energy loss. Meanwhile, the stress might be large at the high charging current density of 60 mA cm^{-2} . It could be high enough to bring about the crack in the anodic deposited layer, resulting in the breaking away of the PbO_x layer into the electrolyte and lowering the energy loss [28].

The cell that was charged to the capacity of 20 mA h at 2.15 V and discharged at 40 mA cm^{-2} until the cell voltage dropped to 0.5 V, was selected to cycle for a long time. The cell was cycled for 261 cycling numbers at a coulombic efficiency of more than 80%. Under potentiostatic conditions, the fluctuation of the charge voltage can be avoided obviously. It guarantees the uniform oxidation activity of PbO_x , the efficiency and cycling stability of the lead methanesulfonate flow battery could be improved. Therefore, by controlling the cell voltage, i.e. the positive electrode potential, the particle size was decreased. The specific surface area of the electrode was increased after the entire electrode was covered with the layer of PbO_x . And also the oxidation activity and conductivity of PbO_x were improved due to the oxidation state of lead ion and the stoichiometry of PbO_x . Meanwhile at the high positive electrode potential, the polarization resistance was decreased to enhance the charge transfer kinetics, favoring the electrode reaction of $\text{PbO}_2/\text{Pb}^{2+}$. With the positive electrode potential increasing, the

content of β -phase decreases, and α -phase's increases. It is likely to optimize the ratio of α -phase/ β -phase to form a thick layer of PbO_x onto the surface of the electrode [9], in which the physicochemical property could be uniform by controlling the positive electrode potential. However, the stress within the PbO_x layer cannot be ignored, especially at the high current density. It could be large enough to bring about the crack of the PbO_x layer, even breaking away of the PbO_x layer from the electrode [28]. A suitable positive electrode potential should be considered, and also a low discharging current density could be another effective method to slowly release the stress. In this work, with the PbO_x layer built up onto the positive electrode during charging, the potential working on the electrodeposition of PbO_x becomes truly lower than the fixed value, such as 1.7 V vs. SCE, due to the resistance of PbO_x layer. In this case, in order to keep the same electrodeposition potential of PbO_x , it will be necessary to set up a relationship between the positive electrode potential and the resistance of PbO_x layer in the future work, especially for the thicker PbO_x layer formed during the charge.

4. Conclusions

The deposition and dissolution of anodic deposited materials is a key factor to improve the efficiency of lead methanesulfonate flow battery. The anodic deposited material is the compound in which oxygen deficiency in PbO_2 . X is introduced to represent the average content of $\text{O}_{\text{lattice}}$ in the anodic materials, PbO_x . The high value of x means the high oxidation activity of the anodic materials, and good conductivity as well. XPS was applied to investigate the content of $\text{O}_{\text{lattice}}$ in PbO_x . The high positive electrode potential is beneficial to enhancing the content of $\text{O}_{\text{lattice}}$. Correspondingly its polarization resistance R_p is low from analyses of EIS. The particle size becomes smaller with the positive electrode potential increasing. By controlling the charge voltage of the cell, the coulombic efficiency of $94 \pm 2\%$ has been achieved for the first 20 cycles under potentiostatic conditions of 2.15 V - 40 mA. After 261 cycles, the efficiency drops below 80%, since the effective electrodeposition potential of PbO_x become lower due to the resistance of PbO_x layer built up on the anode.

Acknowledgements

The authors would like to thank The Key Laboratory Project of Shaanxi Province (17JS084), The Science Fundation of Xi'an University of Science and Technology (101-451016021), Haofa Environmental Protection Technology (Shenzhen) Co., Ltd. for the financial support of the work.

References

- [1] A. Hazza, D. Pletcher, R. Wills, A novel flow battery: a lead acid battery based on an electrolyte with soluble lead (II) Part I. Preliminary studies, *J. Chem. Phys.* 6 (2004) 1773-1778.
- [2] D. Pletcher, R. Wills, A novel flow battery: a lead acid battery based on an electrolyte with soluble lead (II) Part II. Flow cell studies, *J. Chem. Soc. Faraday T* 6 (2004) 1779-1785.
- [3] M. Krishna, E.J. Fraser, R.G.A. Wills, F.C. Walsh, Developments in Soluble Lead Redox Flow Batteries and Remaining Challenges: An Illustrated Review, *J. Power Sources* 15 (2018) 60-90.
- [4] A.B. Velichenko, R. Amadelli, E.V. Gruzdeva, T.V. Luk'yanenko, F.I. Danilov, Electrodeposition of lead dioxide from methanesulfonate solutions, *J. Power Sources* 191 (2009) 103-110.
- [5] A.B. Velichenko, D.V. Girenko, F.I. Danilov, Mechanism of lead dioxide electrodeposition, *J. Electroanal. Chem.* 405 (1996) 127-132.
- [6] A.B. Velichenko, E.A. Baranova, D.V. Girenko, R. Amadelli, F.I. Danilov, Electrodeposition of Co-doped lead dioxide and its physicochemical properties, *J. Electroanal. Chem.* 527 (2002) 56-64.
- [7] J.P. Carr, N.A. Hampson, The impedance of the PbO_2 /aqueous electrolyte interface: II. Phosphate electrolytes, *J. Electroanal. Chem. Interfacial Electrochem* 28 (1970) 65-70.
- [8] I. Sircs, C.T. Low, C. Ponce de León, F.C. Walsh, The Characterisation of Lead Dioxide Electrode Coatings Prepared from Aqueous Methanesulfonic Acid under Controlled Deposition Conditions, *Electrochim. Acta* 55 (2010) 2163-2172.
- [9] X. Li, D. Pletcher, F.C. Walsh, A novel flow battery: A lead acid battery based on an

- electrolyte with soluble lead(II) Part VII. Further studies of the lead dioxide positive electrode, *Electrochim. Acta* 54 (2009) 4688–4695.
- [10] X. Li, D. Pletcher, F.C. Walsh, Electrodeposited Lead Dioxide Coatings, *Chem. Soc. Rev.* 40 (2011) 3879–3894.
- [11] A. Oury, A. Kirchev, Y. Bultel, E. Chainet, PbO₂/Pb₂+ cycling in methanesulfonic acid and mechanisms associated for soluble lead-acid flow battery applications, *Electrochim. Acta* 71 (2012) 140–149.
- [12] D. Pavlov, Semiconductor mechanism of the processes during electrochemical oxidation of PbO to PbO₂, *J. Electroanal. Chem.* 118 (1981) 167–185.
- [13] D. Pavlov, E. Bashtavelova, D. Simonsson, P. Ekdunge, Processes at the micro-level in the oxidation of PbSO₄ to PbO₂ during charging of lead/acid battery positive plates, *J. Power Source* 30 (1990) 77–97.
- [14] D. Pavlov, B. Monahov, G. Sundholm, T. Laitinen, The effect of antimony on the anodic behaviour of lead in H₂SO₄ solution: part II. Dependence of the phase composition of the anodic layer on the oxidation potential, *J. Electroanal. Chem. Interfacial Electrochem* 305 (1991) 57–72.
- [15] D. Pavlov, Reply to comments on “effect of chemisorbed water on the electrical capacity of the lead-acid battery positive plate”, *J. Power Sources* 22 (1988) 179–182.
- [16] H.B. Suffredini, G.R. Salazar-Banda, L.A. Avaca, Enhanced ethanol oxidation on PbO_x-containing electrode materials for fuel cell applications, *J. Power Sources* 171 (2007) 355–362.
- [17] D. Pletcher, R. Wills, A novel flow battery—a lead acid battery based on an electrolyte with soluble lead(II) III. The influence of conditions on battery performance, *J. Power Sources* 149 (2005) 96–102.
- [18] J. Collins, X. Li, D. Pletcher, R. Tangirala, D. Stratton-Campbell, F.C. Walsh, C. Zhang, A novel flow battery: A lead acid battery based on an electrolyte with soluble lead(II). Part IX: Electrode and electrolyte conditioning with hydrogen peroxide, *J. Power Sources* 195 (2010) 2975–2978.
- [19] J.P. Carr, N.A. Hampson, R. Taylor, Fast linear sweep voltammetry studies on polycrystalline lead and electrodeposited lead dioxide (α and β) in aqueous sulphuric acid, *J. Electroanal. Chem. Interfacial Electrochem* 1 (1971) 109–120.
- [20] S.A. Campbell, L.M. Peter, A study of the effect of deposition current density of the structure of electrodeposited α -PbO₂, *Electrochim. Acta* 34 (1989) 943–949.
- [21] V.Y. Zenou, S. Bakardjieva, Microstructural analysis of undoped and moderately Sc-doped TiO₂ anatase nanoparticles using Scherrer equation and Debye function analysis, *Mater. Charact.* 144 (2018) 287–296.
- [22] R.V. Vijayalakshmi, A. Kannan, P.P. Kumar, K. Ravichandran, P. Rajakumar, The role of glycodendrimer in the structural and optical studies of Co@AgCl core-shell nanoparticles, *Mater. Chem. Phys.* 221 (2019) 356–360.
- [23] X. Li, H. Xu, W. Yan, Effects of twelve sodium dodecyl sulfate (SDS) on electrocatalytic performance and stability of PbO₂ electrode, *J. Alloys, Compd.* 718 (2017) 386–395.
- [24] Y. Shi, Y. Huang, C.P. Huang, Oxidation of ammonia in dilute aqueous solutions over graphite-supported a- and b-lead dioxide electrodes (PbO₂@G), *Electrochim. Acta* 257 (2017) 444–454.
- [25] O. Shmychkova, T. Luk'yanenko, R. Amadelli, A. Velichenko, Physico-chemical properties of PbO₂-anodes doped with Sn⁴⁺ and complex ions, *J. Electroanal. Chem.* 717–718 (2014) 196–201.
- [26] X. Duan, F. Xu, Y. Wang, Y. Chen, L. Chang, Fabrication of a hydrophobic SDBS-PbO₂ anode for electrochemical degradation of nitrobenzene in aqueous solution, *Electrochim. Acta* 282 (2018) 662–671.
- [27] J. Collins, G. Kear, X. Li, C.T.J. Low, D. Pletcher, R. Tangirala, D. Stratton-Campbell, F.C. Walsh, C. Zhang, A novel flow battery: a lead acid battery based on an electrolyte with soluble lead(II) Part VIII. The cycling of a 10 cm × 10 cm flow cell, *J. Power Sources* 195 (2010) 1731–1738.
- [28] D. Pletcher, H. Zhou, G. Kear, C.T. John Low, F.C. Walsh, R.G.A. Wills, A novel flow battery—a lead-acid battery based on an electrolyte with soluble lead(II) part VI. Studies of the lead dioxide positive electrode, *J. Power Sources* 180 (2008) 630–634.
- [29] A.A. Shah, X. Li, R.G.A. Wills, F.C. Walsh, A mathematical model for the soluble lead-acid flow battery, *J. Electrochem. Soc.* 157 (2010) A589–A599.